1

Tetraphenylpyrazine-based AIEgens: Synthesis and Applications

Ming Chen[1], Anjun Qin[3], and Ben Zhong Tang[2,3,4]

[1] College of Chemistry and Materials Science, Jinan University, Guangzhou, China
[2] Department of Chemistry, Hong Kong Branch of Chinese National Engineering Research Center for Tissue Restoration and Reconstruction, The Hong Kong University of Science & Technology, Clear Water Bay, Kowloon, Hong Kong, China
[3] State Key Laboratory of Luminescent Materials and Devices, Guangdong Provincial Key Laboratory of Luminescence from Molecular Aggregates, Center for Aggregation-Induced Emission, South China University of Technology, Guangzhou, China
[4] Shenzhen Institute of Aggregate Science and Technology, School of Science and Engineering, The Chinese University of Hong Kong, Shenzhen, Guangdong, China

1.1 Introduction

Luminescent materials have been widely applied in display, illumination, and information transfer, etc [1–3]. However, in real-word applications, they are most employed in the aggregate state (e.g. solid-state-emissive thin film in organic light-emitting diodes (OLEDs) and nanoimaging materials) [4–8]. The traditional chromophores show extremely strong emissions in the solution but exhibit almost quenched emission behavior upon aggregation. For such a reason, scientists are in enthusiastic pursuit of highly efficient luminescent materials in the solid state. One would consider it to be better if the aggregation could be utilized to play a positive instead of a negative role in enhancing luminescence. This idea had come true until 2001 when Tang had a beautiful encounter with aggregation-induced emission (AIE) [9–12]. AIE luminogens (AIEgens) possess the luminescence behavior opposite to the traditional luminogens as their twisted and flexible molecular conformation allows them to dissipate the excited-state energy nonradiatively by molecular motion in the solution, while such motion is suppressed in the aggregate state to open up the radiation channel [13–16]. Thus, the problem of aggregation-caused quenching (ACQ) effect perplexed in traditional dyes has been overcome thoroughly by AIE, and more than 10 000 works aiming at mechanism study, molecular design, and functionality exploitation have been published based on this hot topic.

It is crucial to develop a great variety of AIEgens because molecules with different structures may cause different properties and functions. By choosing suitable AIE archetypal molecules for structural decoration, such a target can be achieved readily. Up to date, dozens of archetypal AIEgens have been developed. Among them, hydrocarbon AIEgens like tetraphenylethene (TPE), triphenylethene, tetraphenyl-1,4-butadiene (TPBD), and distyrylanthracene (DSA) are very popular because they are competent in designing materials with high luminescence efficiencies Chart 1.1 [17–20].So far, TPE is regarded as the most famous AIEgen because it is very easy to synthesize and modify, making that the majority of AIE researches are established based on this system. The mechanism for elaborating AIE phenomenon of TPE is still in debate [21]. The early studies show that the restriction of rotation of peripheral phenyl rings against the central double

Handbook of Aggregation-Induced Emission: Volume 2 Typical AIEgens Design, First Edition.
Edited by Youhong Tang and Ben Zhong Tang.

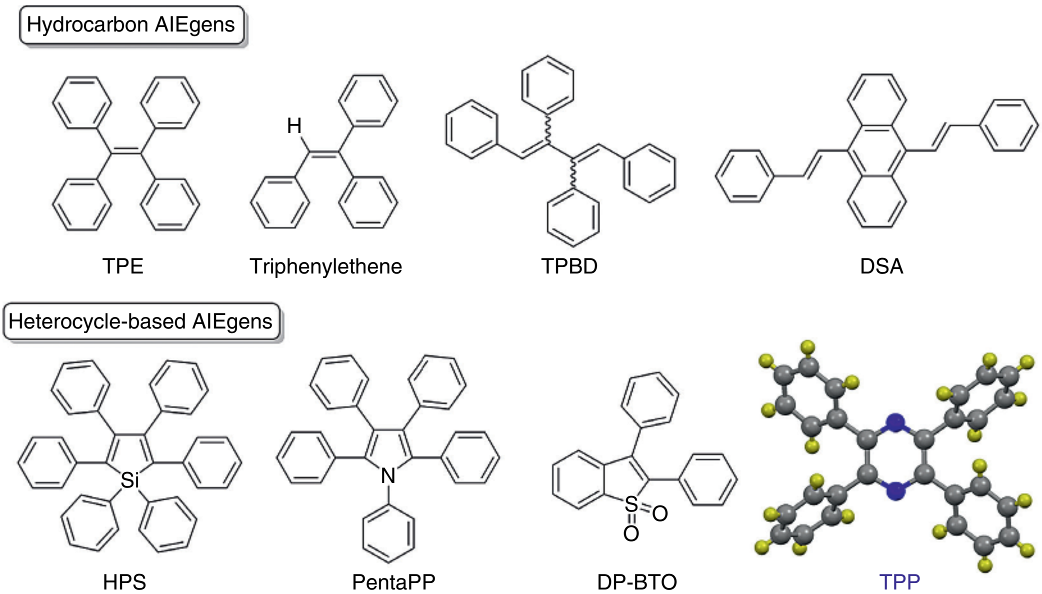

Chart 1.1 Molecular structures of AIEgens of tetraphenylethene (TPE), triphenylethene, tetraphenyl-1,4-butadiene (TPBD), distyrylanthracene (DSA), hexaphenylsilole (HPS), pentaphenylpyrrole (PentaPP), phenyl-substituted oxidized benzothiophene (DP-BTO), and tetraphenylpyrazine (TPP).

bond is the essential cause. Zheng reveals that photoisomerization of the central double bond in TPE plays an important role in quenching its emission in the solution based on the studies of photophysical behaviors of TPEs with its adjacent phenyl rings chemically locked at different sides [22]. In other words, the double bond in TPE is unstable and easy-to-form free radicals under irradiation and heat. On the other hand, Chi observed a photochromism of Cl-substituted triphenylethene as a result of the cyclization reaction taking place between the phenyl rings in the molecule under UV light stimuli [23]. Thus, the stability of AIE materials based on these hydrocarbon AIEgens needs to be considered and improved.

By contrast, no central double bond exists in the heterocycle-based AIEgens, making them free of such trouble. The typical heterocycle-based AIEgens are hexaphenylsilole (HPS), pentaphenylpyrrole (PentaPP), phenyl-substituted oxidized benzothiophene (DP-BTO), and so on Chart 1.1 [24–30]. The introduction of heteroatoms in these AIEgens obviously endows them with different electronic properties. For example, in HPS, the interaction of σ^* orbital of the silicon atom and π^* orbital of the carbon atom enables it to possess low-lying LUMO energy level. It imparts HPS with high electron affinity, which can act as an electron-accepting unit in molecular design and increase the electron-transporting property as material [31]. On the other hand, the orbitals of the nitrogen atom in PentaPP is sp^2-hybridized, while the lone pair electrons occupy the p orbital, which arrays parallelly with the p orbitals from adjacent carbon atoms. It remarkably increases the p–π interaction and makes the central pyrrole ring electron-rich. Some electron-donating and hole-transporting properties of PentaPP are thus obtained in molecular and material designs [32]. However, although these heterocycle-based AIEgens show good photo- and thermal stabilities, their chemical stability should be improved. For example, the silole ring in HPS is easy to decompose under basic atmosphere. Besides, their synthesis is always tedious, the reaction condition is rigorous, and the purification is difficult. Thus, it is urgent to develop new AIEgens in combination with the advantages from the above hydrocarbon and heterocycle ones.

In 2015, Tang reported a heterocycle-based AIEgen, namely, tetraphenylpyrazine (TPP), with its structure possessing four phenyl rings attaching to the central pyrazine heterocycle ring Chart 1.1 [33–37]. The rotation of the peripheral phenyl ring against the pyrazine ring makes the molecule less emissive in the solution. The twisted conformation of TPP prohibits the formation of π–π stacking in the aggregate state, while the multiple intermolecular C–H$\cdots\pi$ interactions exist to lock the molecular motions. These factors collectively contribute to the AIE effect. A more detailed mechanism is still under investigation because the central pyrazine ring is possible to participate in the molecular motions in the excited state. The preparation of TPP is very simple even when compared with that of TPE, and many routes are alternative according to various requirements. The stability of TPP is pretty good due to the whole aromatic structure of the molecule and the high bond energy of the C–N bond in the central heterocycle. Different from pyrrole, the nitrogen atom forms a double bond with one of the neighboring carton atoms in pyrazine. The lone pair electrons, therefore, occupy one of the sp^2 orbitals of the nitrogen atom, which parallels to the pyrazine plane. The interaction of lone pair electrons and π electrons will never occur, whereas the strong electronegativity of the nitrogen atom in C–N bonds induces the polarization of an electron cloud in the ring, which makes the pyrazine ring in TPP electron-deficient [38, 39]. Indeed, by decorating TPP with phenyl rings or weakly electron-donating methoxyl groups, the resulting donor–acceptor (D–A) effect can finely tune the emissions of derivatives in the whole blue light region. These features indicate that the AIE-active TPP is a promising candidate utilized for further development of high-performance materials.

With the development in the last five years, more and more works with TPP as motif have emerged. Firstly, besides the conventional methods, the new methodologies in the preparation of TPP and its derivatives have been established. By using the new catalytic systems, rather high yields (>98%) are obtained in the preparation. A recent work shows that TPP can even be prepared efficiently by direct heating of the starting materials in the solid phase. Secondly, many luminescent applications (e.g. highly efficient OLEDs, gas, explosive, and ion sensors, etc.) based on TPP have been developed. On the other hand, due to the symmetry of TPP, its researches on the reticular chemistry have sprung up. For example, TPP-based organic cage and metal–organic framework (MOF) can be designed easily to exhibit self-assembling and sensing properties. Herein, we summarize recent research efforts on the development of this AIE system, including synthesis and functions, and we hope, with this chapter, new ideas could be stimulated to exploit the advanced functional materials based on TPP.

1.2 Synthesis of TPP-based AIEgens

1.2.1 Cyclization Reaction

Although TPP was found to be AIE-active by Tang in 2015, its research dates back to the mid-nineteenth century. The early synthesis of TPP was carried out by Laurent in 1845 and later by Erdmann in 1865 [40, 41]. The reaction was carried out by heating benzoin with ammonium chloride at 100 °C for four to six hours. Three main products formed after the reaction named as benzoinam (formula $C_{28}H_{24}N_2O$), benzoinimide (formula $C_{14}H_{11}N$), and lophine, respectively. In 1886, Japp and Wilson reinvestigated the reaction. They found that a yellow crystalline powder of benzoinimide formerly obtained was actually impure. After recrystallization with a large amount of alcohol, colorless, slender, and lustrous crystals were collected. Further elemental analysis study indicated that the formula of the compound agreed better with $C_{28}H_{20}N_2$ than with $C_{14}H_{11}N$. That is, the name of benzoinimide given by Erdmann is misleading. They thus renamed the compound as ditolane-azotide and also gave the prototype structure of TPP in the text [42]. It is the first report of TPP.

Since that, the researches on TPP were burgeoning. In 1937, Davidson, Weiss, and Jelling studied the action of ammonia on benzoin [43]. Besides the generated TPP, an imidazole derivative of 2-methyl-4,5-dipenylglyoxaline and tetraphenyldihydropyrazine was formed. It represented the most classical rudiment in the later preparation of TPP. The reaction mechanism was given as below: the carbonyl group of benzoin was possible to convert to imine in the presence of ammonia, followed by generating carbinamine by structural rearrangement, while the hydroxyl group nearby was converted to the carbonyl group. Two formed intermediates can undergo cyclization reaction by condensation and removal of water. After structural tautomerization, a resembling product of tetraphenyldihydropyrazine was formed to oxidize to TPP. On the other hand, the intermediate was also easy to react with the solvent of acetic acid by the amino group and then formed 2-methyl-4,5-dipenylglyoxaline by cyclization (Scheme 1.1). The formation of tetraphenyldihydropyrazine was evidenced by the orange color of the reaction mixture soon after refluxing of the starting materials. Remarkably, oxygen plays a crucial role in the conversion of tetraphenyldihydropyrazine to TPP. It is proved that the yield of reaction solution bubbled with air is higher than that in the closed environment. Nevertheless, the total yield of TPP is in the range from 53 to 57%, and the tetraphenyldihydropyrazine cannot convert to TPP completely even in the presence of enough oxygen. After filtering out the formed crude TPP precipitates, the unreacted tetraphenyldihydropyrazine in the mother liquor can be further oxidized to TPP by adding nitric acid until the orange color of solution was discharged.

Tang also reported the synthesis of TPP by refluxing benzoin, ammonium acetate, and acetic anhydride in acetic acid for 3.5 hours, while the acetic anhydride acts as a dehydrating agent to remove the water after cyclization (Scheme 1.2, Route A, Condition 1) [33]. TPP shows the same polarity with the byproducts as monitored by the silica gel plate. The blue emission of TPP disappeared, while only the orange emission was observed on the plate. It is mainly due to energy transfer taking place from TPP to the byproducts, which dramatically quenches its emission. It implies that the purity of TPP after purification must be rather high because the trace of impurities in TPP will obviously affect its photo-physical properties. TPP and its byproducts show different solubility in acetic acid. TPP is badly dissolved in acetic acid. It precipitates during the reaction, while most of the byproducts were still left in the solution. The crude TPP powder is collected by filtration and

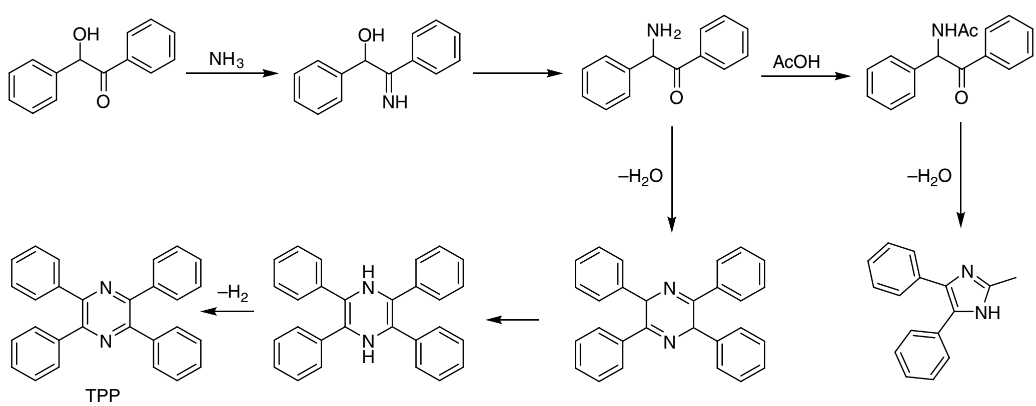

Scheme 1.1 Reaction mechanism of synthesizing TPP with benzoin and ammonia.

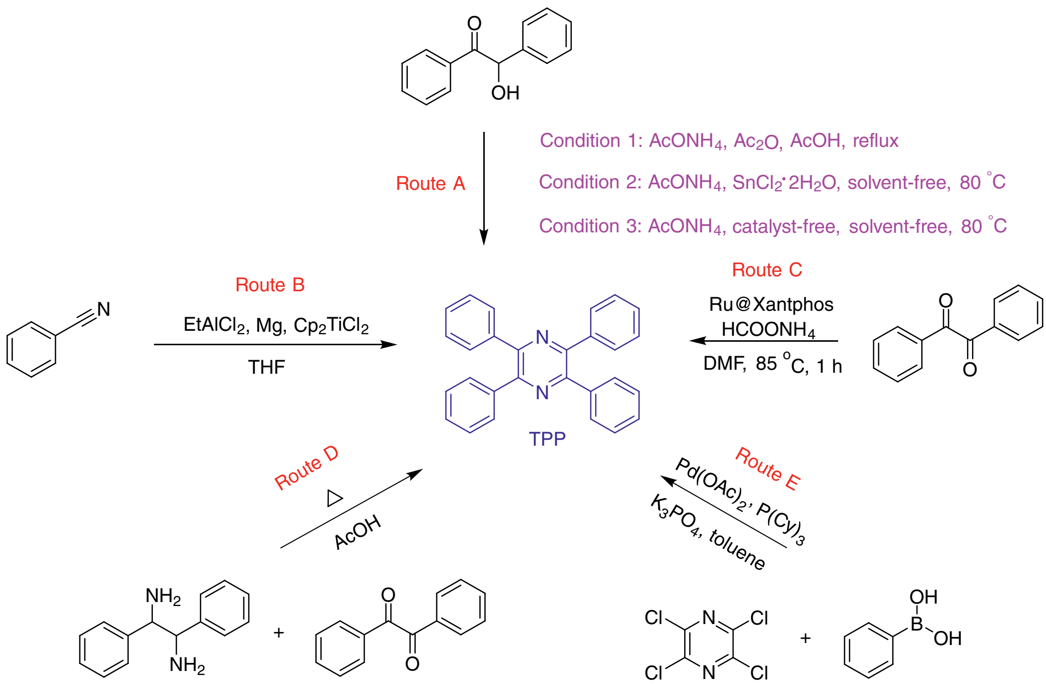

Scheme 1.2 Current synthetic routes to TPP.

shows a yellow appearance due to the presence of trace impurities. However, repeated recrystallization of crude products in a larger amount of heat acetic acid can afford very pure TPP crystals. The yield (34%) is lower than the above studies, probably due to the loss of product during the purification. The convenience in preparation and purification of TPP makes it very promising for further deep investigations.

This method not only affords TPP readily but is also useful for preparing its derivatives with diverse structures. For example, by using mono- or disubstituted benzoin, di- or tetrasubstituted TPP derivatives can be easily obtained. The reaction is less affected by the electronic effect of substituents. However, if the substituents are bulky, the crude products are difficult to purify by recrystallization. It is worth noting that two isomers are usually formed by using monosubstituted benzoin in the reaction. Such behavior is similar to that in the preparation of disubstituted TPE derivatives by the McMurry coupling reaction [44]. The presence of isomerization in TPP derivatives is proved by the fact that four resonance signals exist around 148 ppm in their ^{13}C NMR spectra due to the four different chemical environments of carbon atoms in the pyrazine ring [33].

Tamaddon used $SnCl_2{\cdot}2H_2O$ as a catalyst to synthesize α-amino ketones with benzoin and aniline as starting materials under solvent-free conditions at either 80 °C or microwave irradiation [45]. Although the yields of reaction are high (up to 83%), the undesired byproduct of 1,4-dibenzyl-2,3,5,6-tetraphenyl-1,4-dihydropyrazine is formed as examined by the NMR analysis, which is possibly due to the self-condensation of the in situ formed α-amino ketones. Further investigation indicated that under the same catalytic condition, a [2 + 1 + 1 + 2] four-component reaction of benzoin and ammonium acetate can generate TPP in a high yield of 90% (Scheme 1.2, Route A, Condition 2). It provides a convenient strategy to prepare tetrasubstituted tetraphenylpyrazines in high yields. The substituents on benzoin are widely alternative. For example, by using methoxyl-, methyl-, bromine-, chlorine-, and fluorine-substituted benzoins, the reactions can proceed smoothly. However, as the electron-donating property of substituents increases, the yield of reactions slightly decreases.

Subsequently, Tamaddon found that the multicomponent reaction can be carried out without $SnCl_2{\cdot}2H_2O$ as catalyst (Scheme 1.2, Route A, Condition 3) [46]. That is, $SnCl_2{\cdot}2H_2O$ is not necessary in the reactions. By directly heating the solid mixture of benzoin and ammonium acetate at 80 °C, the product can be obtained in a very high yield. Overall, this reaction is very close to the original one reported by Laurent, Erdmann, Japp, and Wilson, except that the ammonium chloride has been replaced by ammonium acetate. This optimal reaction condition was confirmed by the author after evaluation of the influence of ammonium salt, solvent, and reaction temperature on the reaction efficiency. The yields remain high in the reaction of benzoin derivatives regardless of the electron effect of the substituents. The reaction mechanism was similar to the previous one. Ammonium acetate releases the ammonia by heating to react with benzoin to generate an intermediate. Because the ammonium acetate is subtly excess, few acetic acid is formed, which can hardly react with the intermediate to produce 2-methyl-4,5-dipenylglyoxaline. On the other hand, the solid-state reaction allows the full contact of reactant with air. Both the factors may decide a high yield of reaction.

Khafizova reported a new one-pot synthesis of tetrasubstituted TPP derivatives based on the reaction of nitriles with $EtAlCl_2$ catalyzed by metallic Mg and Cp_2TiCl_2 (Scheme 1.2, Route B) [47]. The reaction is efficient, and the product can be obtained in good yields of 60–90%. The catalytic system of Ti and Zr complexes such as Cp_2TiCl_2, $Ti(Pr^iO)_4$, $TiCl_4$, $Cp_2Ti(PMe_3)_2$, $Ti(acac)_2Cl_2$, $Ti(Net_2)_4$, and Cp_2ZrCl_2 is investigated to examine the influence on the reaction. Only Cp_2TiCl_2 and $Ti(Pr_iO)_4$ display superior catalytic activity and selectivity. Besides, the reaction has a wide universality of nitriles. For example, by using the starting materials of 2-methyl-, 3-methyl-, 4-methyl-, 4-isopropyl-, 3,5-dimethyl-, and 4-methoxy-substituted benzonitriles, different TPP derivatives with the tetrasubstituents can be obtained efficiently. The probable mechanism of this reaction was also given. Cp_2TiCl_2 was first reduced to the coordinatively unsaturated $Cp_2Ti(II)$ complex by activated Mg. Then, two nitriles can coordinate with the $Cp_2Ti(II)$ complex to form titanium-nitrile π-complexes, followed by transforming to diazatitanacyclopentadiene intermediate A. Subsequently, two additional nitrile molecules are inserted into the active Ti–N bonds of the intermediate, which gives rise to ring expansion to form the unsaturated tetraaza derivative B. The excess $EtAlCl_2$ reacts with B to replace the metal center to generate intermediate C, which further results in TPP by skeletal isomerization after elimination of aluminadiazirine (Scheme 1.3).

Catalytic system based on ruthenium chemistry has been widely investigated because it plays an important role in arene hydrogenation, hydrogenation of carbonyl compound, click reaction, and so on. Leeuwen employed ligand-modified ruthenium nanoparticles (RuNPs) to catalyze the transfer hydrogenation of α-diketone. Interestingly, the unexpected product of TPP was produced by reacting the mixture of benzyl and ammonium formate in dimethyl formamide (DMF) at 85 °C with dbdocphos-stabilized RuNPs as catalyst (Scheme 1.2, Route 3) [48]. A very high yield (>98%) of product was monitored by GC analysis, and the byproducts are water, carbon dioxide, and dihydrogen. However, the reaction affords another product of triphenyloxazole in a yield of 30% in the absence of catalyst, proving that the Ru-based catalyst is indispensable in the reaction process. Besides dbdocphos, other phosphines such as dppp, DPEphos, and Xantphos are also used to prepare RuNPs. Among these, Xantphos-supported RuNPs behave similarly to the dbdocphos-based catalyst in activity and selectivity. The influence of nitrogen source on the reaction was studied. By replacing ammonium formate with ammonium acetate, ammonium chloride, and aqueous ammonia solution, no product of TPP can form, whereas, in the first case, only triphenyloxazole in a 30% conversion is obtained. The efficient catalytic system also has good group tolerance to provide

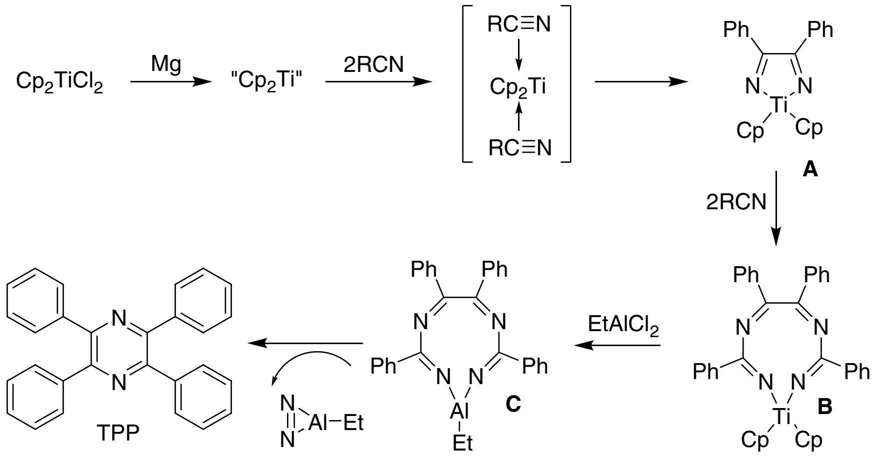

Scheme 1.3 Proposed mechanism of synthesizing TPP catalyzed by Mg and Cp_2TiCl_2.

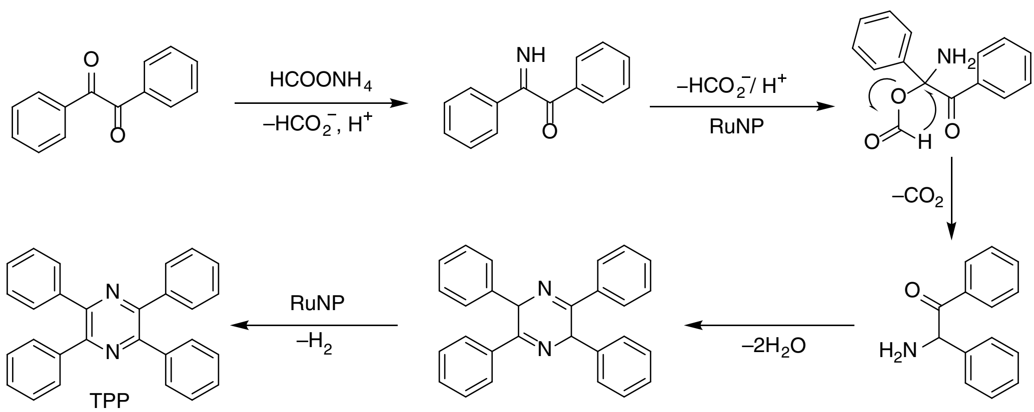

Scheme 1.4 Proposed mechanism of preparing TPP catalyzed by RuNPs.

tetrasubstituted TPP derivatives with different structures. The proposed mechanism of the reaction assumes that the benzyl first undergoes reductive amination under transfer hydrogenation conditions to generate α-amino ketone with RuNPs as catalyst. Then, the molecule self-condenses by removing the water, followed by tautomerization and oxidation to give TPP (Scheme 1.4).

Different from the above reactions, benzil can directly react with dipenylethylenediamine in acetic acid under reflux for four hours to afford TPP (Scheme 1.2, Route 4) [33]. The product was obtained in a satisfactory yield of 47% after recrystallization. A large amount of benzil derivatives with mono- or disubstituents can be prepared readily or purchased at low cost. However, the synthesis and purification of dipenylethylenediamine derivatives are difficult. Thus, this method is very helpful to prepare mono- or disubstituted tetraphenylpyrazines.

1.2.2 Suzuki–Miyaura Reaction

Normally, tetraphenylpyrazines are prepared by cyclization reaction with benzoin and benzil, etc, as starting materials, and nearly all the structures can be designed based on the above routes.

However, Langer reported a new route to synthesize tetrasubstituted tetraphenylpyrazines by the classical Suzuki–Miyaura reaction (Scheme 1.1, Route 5) [49]. In this case, the molecules are prepared by the carbon–carbon coupling of tetrachloropyrazine and arylboronic acid with palladium complexes, phosphorus compounds, and potassium phosphate as catalyst, ligand, and base, respectively. It is probably due to the withdrawing property of central pyrazine that increases the reactivity of peripheral chlorine. Compared with $Pd(PPh_3)_4$, $Pd(OAc)_2$ shows a higher catalytic activity. By applying $Pd(OAc)_2$ as catalyst, choosing different ligands like S-phos, CataCXium, and tricyclohexylphosphine exhibits similar reaction efficiency. The university of arylboronic acids is extremely wide, while the electronic effect of substituents and the steric effect exert less influence on the reaction reactivity.

The tetrachloropyrazine is prepared by heating a mixture of glycine anhydride, PCl_5, and $POCl_3$ at 120 °C. Most of the starting materials are toxic, and the purification process after the reaction is difficult. Although the tetrachloropyrazine is commercially available, the cost is relatively high. It is thus considerable to choose this method for preparation. However, it possesses some difference when compared with the above reactions. For example, it is almost impossible to synthesize tetraldehyde-substituted TPP with the cyclization reaction. By contrast, reacting tetrachloropyrazine with 4-formylphenylboronic acid by the Suzuki–Miyaura reaction may afford the product readily.

1.3 Functionalities of TPP-based AIEgens

TPP is easy to synthesize and modify. In association with its AIE activity, many luminescent functionalities based on tetraphenylpyrazines have been developed. Herein, we will give some examples of their development in OLEDs, bio- and chemosensors, self-assembled materials, and MOFs, etc.

1.3.1 Organic Light-emitting Diodes

TPP is electron-deficient and shows emissions around 400 nm, which is helpful for designing blue emission materials by further structural decoration. When TPP is modified by the strong electron-donating triphenylamine group, a derivative of TPP–TPA is obtained (Chart 1.2). TPP–TPA shows a twisted intramolecular charge transfer (TICT) effect in the polar solvents, while the AIE effect was activated in the aggregate state. The photoluminescence (PL) studies of TPP–TPA indicate that it emits at 455 nm at powder state with an absolute quantum yield (Φ_F) of 35.2% recorded by the integrating sphere. Since the AIE materials are competent to act as luminescent materials to fabricate highly efficient nondoped OLEDs, it is thus very promising to utilize this material for blue OLED fabrication. A typical triple-layer device with a configuration of ITO/NPB

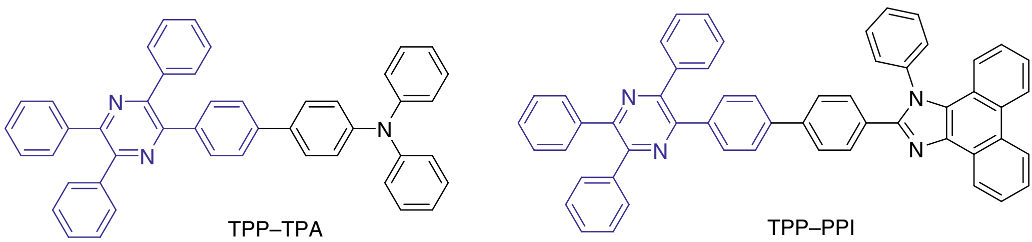

Chart 1.2 Molecular structures of TPP–TPA and TPP–PPI.

Table 1.1 EL performance of devices.

	λ_{EL} (nm)	$V_{on}{}^{a}$ (V)	$L_{max}{}^{b}$ (cd/m^2)	$\eta_C{}^{b}$ (lm/W)	$\eta_P{}^{b}$ (lm/W)	EQE^{b} (%)	CIE $(x, y)^{b}$
TPP–TPA (I)	482	3.7	17 459	5.49	3.18	2.88	—
TPP–TPA (II)	472	2.8	19 170	6.57	6.55	4.08	0.15, 0.21
TPP–PPI	474^{c}	2.9	16 460	8.34	8.18	4.85	0.16, 0.23^{c}

[a] V_{on} = turn-on voltage at 1 cd/m^2.
[b] The maximum luminescence (L_{max}), current efficiency (η_C), power efficiency (η_P), and external quantum efficiency at the maximum values for the devices.
[c] Data recorded at a luminescence of 1000 cd/m^2.

(60 nm)/TPP–TPA (20 nm)/TPBi (40 nm)/LiF (1 nm)/Al is designed, while ITO, NPB (*N*,*N*′-di(1-naphthyl)-*N*,*N*′-diphenyl-benzidine), TPBI (1,3,5-tri(1-phenyl-1*H*-benzo[d]imidazol-2-yl)phenyl), LiF, and Al are used as anode, hole-transporting layer, electron-transporting layer, electron-injecting layer, and cathode, respectively. The device emits at 482 nm with a turn-on voltage (V_{on}), a maximum luminescence (L_{max}), and an external quantum efficiency (EQE) of 3.7 V, 17 459 cd/m^2 and 2.88%, respectively (Table 1.1, Device I). Although a high-lying highest occupied molecular orbital energy level (−5.04 eV) of TPP–TPA is evaluated by cyclic voltammetry, a simplified double-layer device without the hole-transporting layer (TPP–TPA is expected to act as both light-emitting and hole-transporting layers) does not show an improved device performance [50].

It was later reported that TPP derivatives with a D–A structure possess a planarized intramolecular charge transfer (PLICT) effect in the excited state in the polar media. For example, the Φ_F of TPP–TPA in toluene, ethyl acetate, dichloromethane, and DMF changes from 22.7, 50.9, 80.7 to 80.9% as the polarity of the solvent increases. It is due to the formation of planarization conformation or quinone conformation with a good conjugation in the excited state to increase the probability of transition. In that work, another TPP–TPA-based blue OLED (configuration: ITO/HATCN (5 nm)/TAPC (40 nm)/TCTA (5 nm)/TPP–TPA (20 nm)/Bepp2 (45 nm)/Liq (2 nm)/Al) is fabricated with HATCN (2,3,6,7,10,11-hexacyano-1,4,5,8,9,12-hexaazatriphe-nylene), TAPC (1,1-bis(4-di-*p*-tolylaminophenyl)cyclohexane), TCTA (4,4′,4′′-tri-9-carbazolytriphenylamine), and Bepp2 (bis(2-(2-hydroxyphenyl)-pyridine)beryllium) functioned as hole-injecting layer, hole-transporting layer, hole-transporting and electron-blocking layer, and electron-transporting and hole-blocking layer, respectively. However, a very good device performance with V_{on}, L_{max}, and EQE of 2.8 V, 19 170 cd/m^2, and 4.08%, respectively, is obtained (Table 1.1, Device II) [51].

The PLICT effect also takes places in phenanthroimidazole derivative-modified TPP (TPP–PPI), though the phenanthroimidazole-based group is not so electron-donating (Chart 1.2). TPP-PPI shows the AIE effect in THF/water mixtures and emits at 470 nm in the film with Φ_F of 28.1%. While fabricating it into the device with a configuration of ITO/HATCN (5 nm)/NPB (40 nm)/TcTa (5 nm)/TPP–PPI (20 nm)/TPBi (40 nm)/LiF (1 nm)/Al, an excellent device performance of V_{on} (2.9 V), L_{max} (16 460 cd/m^2), and EQE (4.85%) is achieved. It is worth noting that the theoretical limit of EQE of OLEDs fabricated with typical fluorescent materials is 5%. Thus, it demonstrates the huge potential of developing OLEDs with TPP-based luminescent materials [52].

1.3.2 Fluorescent Sensors

Hydrogen sulfide (H_2S) is a natural gas with a rotten egg smell. It is poisonous, corrosive, and flammable. Exposure of H_2S with a small amount can give rise to headache, dizziness, and even death. On the other hand, H_2S is an indispensable endogenous gas in human body by metabolism. It is related to different physiological processes like cell growth, vasodilation, regulation of inflammation, and so on. The abnormal level of H_2S is associated with symptoms such as Alzheimer's diseases and diabetes [53].

Tang synthesized an AIEgen of malonitrile-functionalized TPP (TPP-PDCV) to act as a ratiometric fluorescent probe to detect H_2S with high sensitivity and good selectivity [54]. TPP-PDCV shows an orange emission at 565 nm in the DMSO/PBS buffer mixture (v/v = 9 : 1) due to the TICT from the TPP part to the strong electron-withdrawing malonitrile group. However, upon addition of NaHS, the orange emission disappears gradually, whereas a blue emission centered at 429 nm in the short-wavelength region enhances accordingly. Such a fluorescent response (I_{429}/I_{565}) to H_2S changes less until 10 minutes, indicating that the detection is efficient and can be finished in 10 minutes (Figure 1.1). It is due to the activity of the double bond in the malonitrile group, which can undergo nucleophilic addition by H_2S. Thus, the double bond is easy to break to prohibit the TICT effect. On the other hand, TPP-PDCV is transformed to a thiol-substituted TPP derivative (TPP-PSH) after addition and elimination reactions, which continues to oxidize to form the dithio-containing derivative of TPP-2PS. Because the resulting TPP-2PS shows a lower polarity and lager

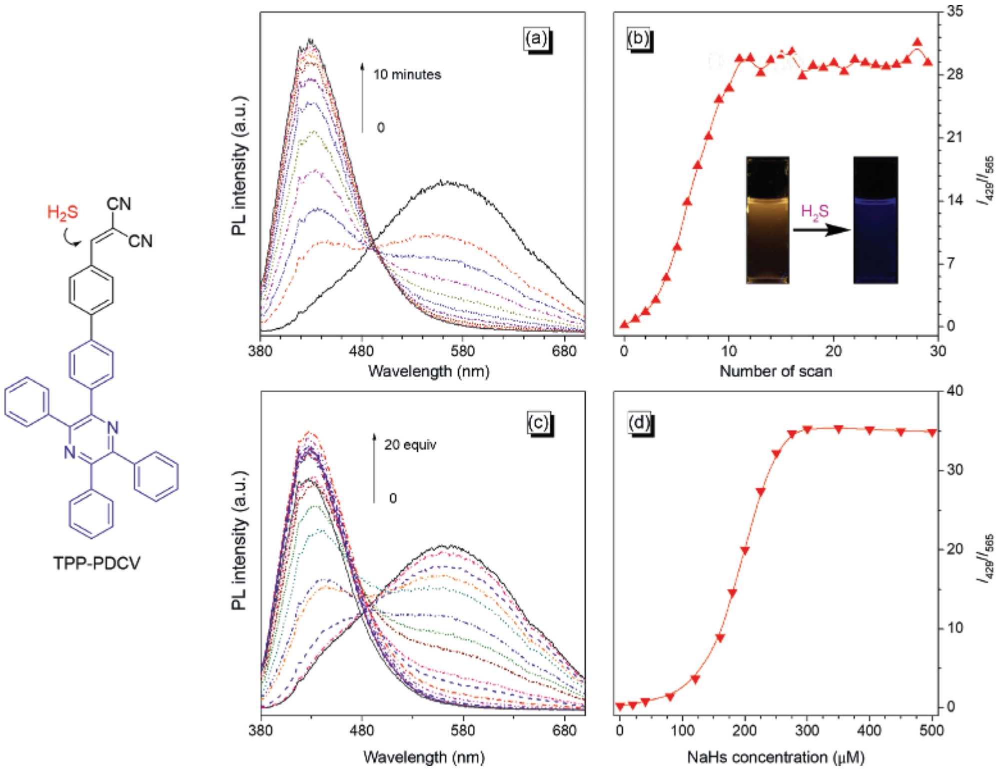

Figure 1.1 Fluorescent detection of H_2S by TPP-PDCV. (a) Time-dependent PL spectra of TPP-PDCV (25 μM) in the DMSO/PBS buffer mixture (v/v = 9 : 1) in the presence of NaHS (250 μM). (b) Plot of the relative PL intensity (I_{429}/I_{565}) versus the number of scan in 25 minutes, where I_{429} and I_{565} are the PL intensity at 429 and 565 nm, respectively. Inset: the photographs of the TPP-PDCV solution before and after the addition of NaHS taken under an irradiation of a 356 nm UV light. (c) PL spectra of TPP-PDCV in the DMSO/PBS buffer mixture (v/v = 9 : 1) with different NaHS concentrations (0–500 μM). (d) Plot of the relative PL intensity (I_{429}/I_{565}) versus NaHS concentration. For all the tests, the excitation wavelength is 372 nm.

rigidity, it displays a bad solubility in the DMSO/water mixture. The TPP-2PS is easy to aggregate to produce a blue light signal contributed by the TPP unit.

The sensor can analyze the H_2S quantificationally. For example, the sensor possesses a response with the NaHS concentration range from 0 to 250 μM. However, in the concentration range of 0–75 and 150–225 μM, the linear responses can be observed, thus providing a platform to detect H_2S at low concentration (Figure 1.1). Besides, the sensor shows a good selectivity against other anions (e.g. AcO^-, F^-, ClO^-, IO_4^-, N_3^-, NO_2^-, and OH^-, etc.), except for CO_3^{2-}, which exerts subtle effect on the detection. The biothiols of cysteine, homocysteine, and glutathione also pose some effect because of the presence of thiol in the structures. However, such an influence can be neglected in comparison to the strong signal in the presence of H_2S.

Study on the influence of molecular structure on the sensing property is particularly valuable to provide the clues for designing advanced functional materials. With this regard, Tang prepared three conjugated isomers of TPP-*p*-TPE, TPP-*m*-TPE, and TPP-*o*-TPE by connecting TPP and triphenylethene at the para-, meta-, and ortho-positions, respectively (Figure 1.2a) [55]. The isomers show the AIE effect due to the melding of the typical AIEgens of TPP and triphenylethene in the structures. Their conformations evolve from an extended to a folded one due to the different linkages between two units, which makes the emissions blue-shifted and luminescence efficiency to decrease gradually. It is reasonable because the molecular conjugation gets worse as the structure changes.

Interestingly, TPP-*o*-TPE is an easy-to-form organic porous crystal thanks to its fold conformation locked by the strong intramolecular C–H···N hydrogen bond. It is an easy-to-form DCM-captured porous crystal (Figure 1.2b). In the crystal, every four molecules coordinately generate a cylinder-like pore with a volume of around 0.27 nm^3, which is enough for accommodating two DCM molecules. The pores are distributed uniformly in the crystal and connected in a straight line as long-ranged nanochannels. The porous crystal produces a fixed framework structure regardless of the guest molecules. For example, each pore can also capture two THF molecules, with the structure of crystal less changed (Figure 1.2c). However, the size of the pore is tunable to fit different volumes of guest molecules.

Considering the difference in the influence of molecular conjugation and porosity caused by the isomerization effect, it is desirable to investigate their sensing behavior. 2,4,6-Trinitrophenol (picric acid, PA) is chosen as the first analyte because it is a well-known model explosive and the accurate detection of explosive meets current needs in antiterrorist and protection of country safety. The detection is basically carried out with the nanoaggregates in solution because of the strong emissions of AIE isomers in the aggregate state. Upon addition of PA, the isomers show similar quenching behavior as the concentration of PA increases. The lifetime of the three sensors has a negligible change before and after analyte addition, demonstrating that a static quenching model dominates the sensing mechanism. Since the process normally takes place from the ground state of isomers to the excited state of PA, no excited-state behaviors of sensors such as fluorescence resonance energy transfer (FRET) and photoinduced electron transfer (PET) will occur, while the interaction between the sensor and the analyte plays a crucial role. Overall, the quenching effect of TPP-*p*-TPE is somewhat higher than those of the others at high PA concentration. It is due to the stronger Lewis acid–base interactions preferred to take place between PA and AIE isomers with better conjugation. On the other hand, although TPP-*o*-TPE possesses the worst molecular conjugation, its quenching effect is a bit larger than TPP-*m*-TPE at a PA concentration of 400–500 μM, which is because of its best porosity that increases the binding capacity between TPP-*o*-TPE and PA. Therefore, both factors collectively determine the detection of PA by nanoprobes (Figure 1.2d).

The study is then focused on the sensing of another analyte of Ru^{3+} by the nanoaggregates because it is important in catalysis but harmful to the environment and toxic to the human beings

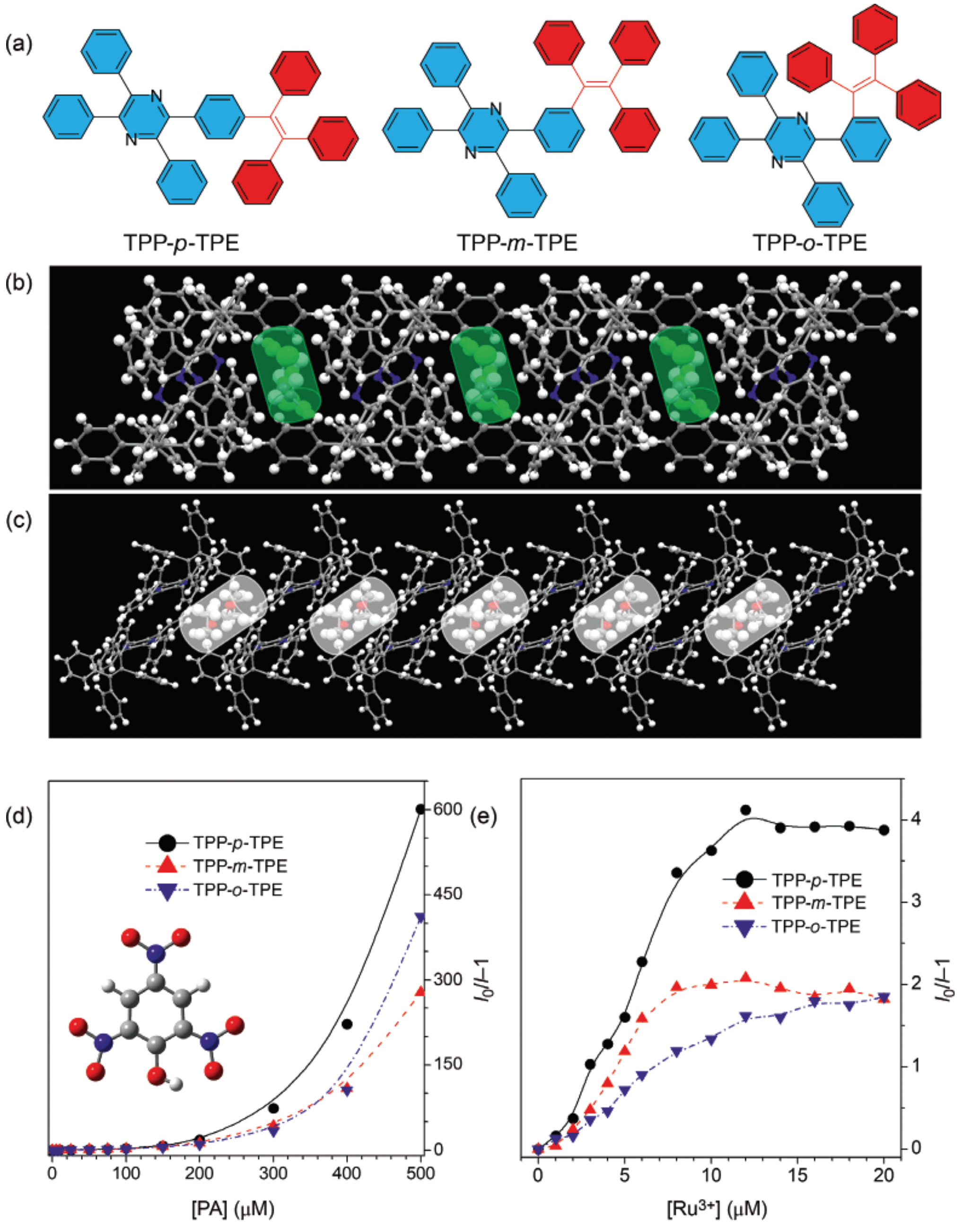

Figure 1.2 Fluorescent detection of PA and Ru^{3+} by AIE isomers. (a) Molecular structures of AIE isomers. (b) DCM- and (c) THF-containing organic porous crystals of TPP-*o*-TPE. (d) Plots of I_0/I-1 versus PA concentration. Inset: molecular structure of PA. (e) Plots of I_0/I-1 versus Ru^{3+} concentration. Inset: molecular structure of PA. In (d) and (e), I_0 and I are the peak intensity of probes before and after the addition of analytes, respectively, and the excitation wavelengths of TPP-*p*-TPE, TPP-*m*-TPE, and TPP-*o*-TPE are 350, 336, and 332 nm, respectively.

(Figure 1.2e) [55]. Different from the above research, the isomers show a partial quenching behavior upon addition of Ru^{3+}. The quenching keeps linear at a low-concentration range of Ru^{3+} and reaches plateaus at high concentrations. Besides, the quenching constant of TPP-*p*-TPE, TPP-*m*-TPE, and TPP-*o*-TPE increases accordingly. The lifetime study indicates that an obvious decrease of lifetime of sensors is observed after addition of Ru^{3+}. Thus, the quenching mechanism is mainly ascribed to a dynamic (collisional) quenching model, which requires a close contact of the excited molecules and the analyte. The Dexter energy transfer is dominated because a short distance of the donor and the acceptor may help the electron exchange between them. On the other hand, the possible influence of FRET on the sensing is ruled out because all the emissions should be quenched if it exists. It seems that the change of the quenching constant of the sensors is related to the variation in the PL quantum efficiency of isomers. It is more likely that the interaction of the isomers and Ru^{3+} plays a major role and a much strong interaction will be produced between Ru^{3+} and isomers with better conjugation.

Although the quenching efficiency of TPP-*m*-TPE is larger than that of TPP-*o*-TPE at low concentrations, it displays the same quenching extent at high concentrations. As the TPP-*o*-TPE is an easy-to-form pore in the aggregates, the sensor will encapsulate more Ru^{3+} into the nanoaggregates, which will enhance their interactions. On the other hand, the presence of 3D voids in the probes may help Ru^{3+} to diffuse and contact more fluorogens to annihilate the emission. Both factors enable the TPP-*o*-TPE to possess similar quenching extent with TPP-*m*-TPE, while the plateaus of the former will be reached at a higher Ru^{3+} concentration. However, the isomerization effect has less influence on the selectivity of the sensors.

For examples, by addition of other metal ions like Ag^{+}, Fe^{3+}, and Cu^{2+}, etc., no fluorescent response can be observed.

1.3.3 Chiral Cage for Self-assembly to Achieve White-light Emission

Organic cage compounds have drawn considerable attention due to their wide functionalities in self-assembly, gas adsorption, and catalysis, etc [56]. Currently, the organic cages are basically designed based on the classical organic reactions of specific building units. The conjugated units are promising in organic cage design, and the study of optical properties of organic cage is attractive by introduction of these units. However, most of the conjugated units possess ACQ effect. There are few studies on AIE unit-based organic cages because of lack of AIE prototype structures with good symmetry for design.

As we know, TPP is an AIEgen with four peripheral phenyl rings symmetrically attached to the central pyrazine. Thus, utilization of TPP to develop a luminescent cage is very promising. Tang reported the synthesis of an amphiphilic organic cage with tetrahydroxyl-substituted TPP (TPP-4OH) and substituted 2,6-dichloro-1,3,5-triazine (Figure 1.3a) [57]. TPP-4OH shows very weak emission in the solution due to the vigorous molecular motion under excitation. However, the TPP cage shows a strong emission at 397 nm with a Φ_F of 34.3% (Figure 1.3b). Theoretical studies reveal that the rotational energy barrier for the phenyl rings' flipping in the TPP cage is much larger than that in TPP-OH, which is due to the congested array of each unit in the cage. As the motion of TPP is greatly prohibited in the cage, TPP cage thus exhibits strong emission by suppressing the nonradiative transition. This study also verifies that the restriction of molecular motion is the cause of the AIE effect.

The studies of chirality are closely related to medicinal chemistry and 3D organic electronics. So far, the introduction of a chiral carbon atom into the structure can be regarded as the main source in designing chiral compounds. Interestingly, the TPP cage here also possesses a chirality though

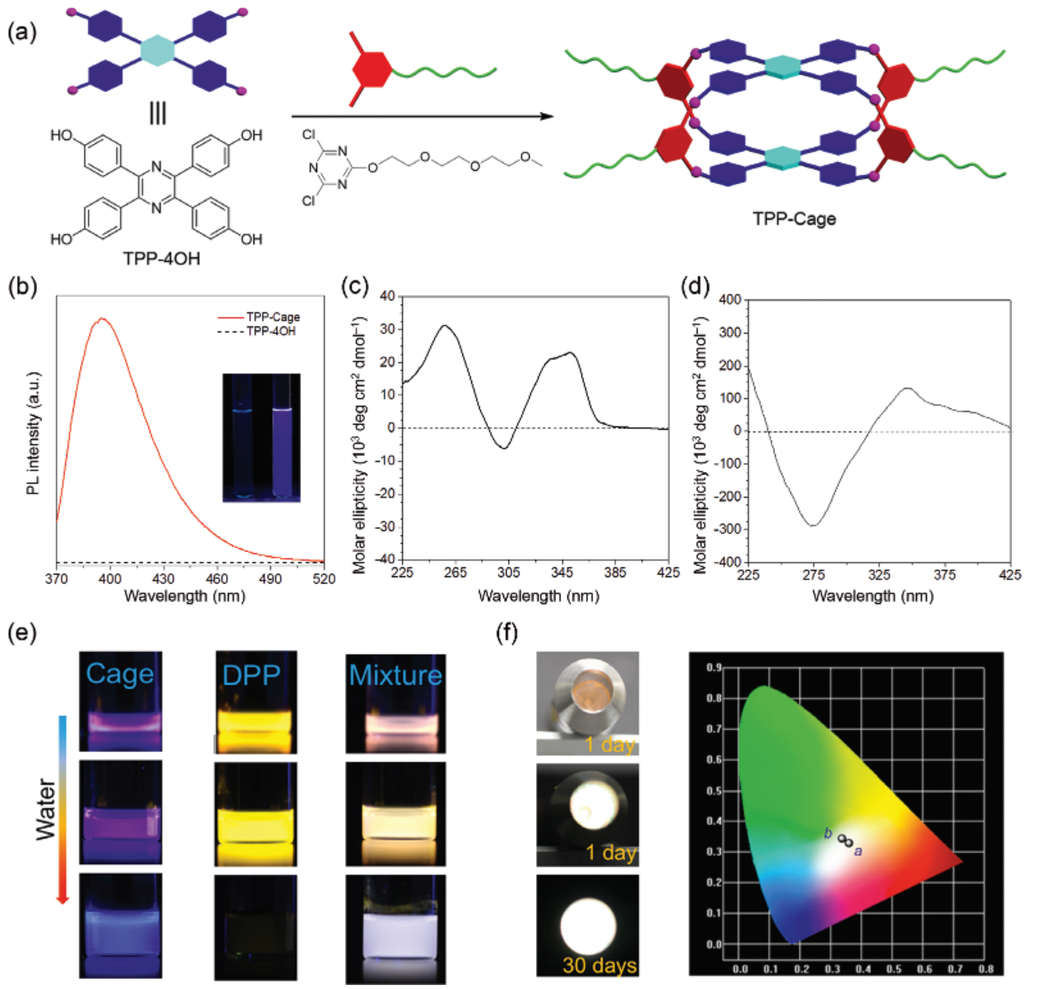

Figure 1.3 TPP-based chiral cage for self-assembly to achieve white-light emission. (a) Synthetic route to the TPP cage. (b) PL spectra of TPP-4OH and TPP cage in THF; their concentration is 50 μM. Inset: their photographs taken under a UV light irradiation. CD spectra of the TPP cage in (c) acetonitrile and (d) acetonitrile/water mixture with a 95% water content; the concentration is 100 μM. (e) Photographs of the TPP cage, DPP, and complex in THF and THF/water taken under a UV light irradiation. (f) Photographs of the complex-doped PEG film-casted flashlight during different times and the CIE coordinate of its emission spectra.

no chiral carbon atom is incorporated. Circular dichroism (CD) spectroscopy indicates that a Cotton effect occurs in the absorption regions of the phenyl rings and TPP units in both the solution and aqueous suspensions (Figure 1.3c, d). It is due to the clockwise or anticlockwise rotation of the phenyl rings of TPP against the pyrazine ring caused by the steric effect. Such a special molecular conformation enables it to possess mirror asymmetry to show chirality. Theoretically, the TPP cage with the clockwise or anticlockwise propeller is often obtained in a ratio of 1 : 1 after synthesis, and the resulting racemic mixture should quench the chirality. The reason for inducing chirality awaits further investigation. On the other hand, only a stable right-handed crystal can be obtained in the air, which shows a positive Cotton effect that originates from the crystallization-induced asymmetric transformation by destroying the mirror symmetry. Moreover, the CD signals of the TPP cage in the aggregates are much larger than those in the solution, indicative of an aggregation-induced chirality that has rarely been reported.

Obviously, the TPP cage has a hydrophobic cavity and is potential to capture the guest molecules. Thus, the investigation of its host–guest chemistry is expected. Diketopyrrolopyrrole (DPP) is an ACQ chromophore with a yellow emission in the solution. However, the size of DPP can fit the cavity volume of the TPP cage properly and the supramolecular assembly complex between them can be obtained readily. The successful formation of the complex is proved by the NMR titration and analysis, and the UV–vis spectra indicate a complex ratio of 1 : 1. As DPP has an ACQ effect, its emission is easy to be quenched once aggregated. However, DPP shows a strong yellow emission in the cage even when the complex is in the aggregate state (Figure 1.3e). It demonstrates that the DPP molecules have been isolated by the TPP cage while the π–π stacking has been prohibited to overcome the ACQ effect, therefore providing a flexible strategy to design highly efficient solid-state luminescent materials with ACQ luminophores. On the other hand, the strong blue emission of the TPP cage sustains. The combined emissions of blue and yellow lights can be observed in the assembly. The emissions of the complex change somewhat from the solution state to the aggregate state. For example, it shows a pink emission in THF. Upon addition of water, the spectrum shifts to white light, which is probably to the subtle variation in emissions of the TPP unit and DPP by changing the microenvironment. Finally, Tang also demonstrates its potential application as white-light emitters. By doping the complex in the PEG with a weight ratio of 1%, a white-light-emissive PEG film can be formed. Further casting the film onto the UV flashlight gives a stable white-light source for illumination (Figure 1.3f).

1.3.4 Metal–organic Framework

MOFs are a kind of organic–inorganic crystals that consist of metal ions and organic molecules as center and ligand, respectively. The two- or three-dimensional rigid framework makes them porous with a large specific surface area and tunable pore size, thus very promising for utilization as porous materials [58]. MOFs can also be developed as luminescent materials because of their potential luminescent properties of metal ions and ligands. Recently, some luminescent MOFs with TPE-based units as ligand have been designed to exhibit sensing and photocatalytic behaviors [59, 60]. As TPP shows the similar structural symmetry to TPE, TPP-based MOFs are thus desired to be developed.

Yin developed MOFs with Ln^{3+} ions, including Eu^{3+}, Tb^{3+}, and Gd^{3+} as centers and tetracarboxyl-substituted TPP (TPP-4COOH) as ligand [61]. The coordination process can proceed in the mixed solution and be monitored by turn-on emission, indicative of a coordination-induced emission. However, different ion centers may cause different optical properties of MOFs (Figure 1.4a). Eu^{3+}-MOF possesses obvious dual emissions at around 420 and 630 nm, which are originated from the TPP unit and Eu^{3+}, while only the emission of TPP can be observed in Gd^{3+}-MOF. The emission of Tb^{3+} in Tb^{3+}-MOF in the long-wavelength region is weak but still can be discerned. This is due to the different energy gaps between the singlet state and triplet state of a ligand and the triplet state of a ligand and the excited state of metal ions, which determines the different intersystem crossing and sensitization efficiencies (Figure 1.4a). In other words, the emission of metal ions is influenced by the combined consideration of the orbital properties of both metal centers and organic ligands.

Although the various metal ions have been employed, their MOFs show similar structural morphologies as revealed by PXRD analysis, indicative of the university of choosing TPP to design MOFs. Moreover, the emission of the TPP unit in MOFs is somewhat blue-shifted than those of

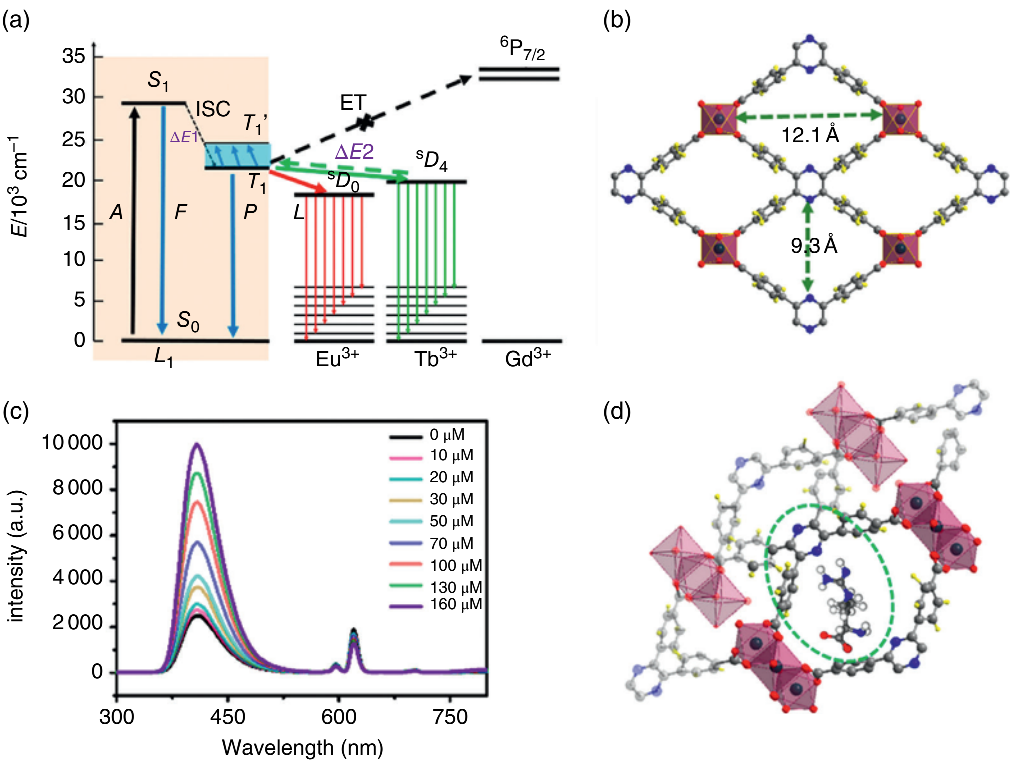

Figure 1.4 Functional MOFs with TPP-4COOH as ligand for sensing. (a) Intersystem crossing and sensitization effect determined by the energy level properties of ligands and metal ions. (b) Crystal structure of Eu^{3+}-MOF. (c) PL spectra of Eu^{3+}-MOF upon the addition of arginine with different concentrations. (d) Model of hydrogen formation between MOF and arginine.

TPP-4COOH. As the formation of MOF can be regarded as a crystallization process, TPP must adjust the conformation to fit the crystal lattice, while a much twisted molecular structure will shorten the conjugation to blue-shift the emission, which is in accordance with the results obtained by the single-crystal diffraction analysis (Figure 1.4b). On the other hand, the Φ_F of TPP-4COOH was measured to be 12.9% in the solid state. However, after being introduced into MOF, the Eu^{3+}-MOF shows dual emissions with a remarkably increased Φ_F of 60.8%. It demonstrates a useful strategy to construct highly efficient luminescent materials by utilizing coordination-induced emission and antenna effect.

As two fluorescent channels are observed in the Eu^{3+}-MOF, it is potential to develop a ratiometric fluorescent probe based on it. Interestingly, Eu^{3+}-MOF has a fluorescent response to arginine, which is an essential amino acid in the body associated with a variety of diseases like cardiovascular and cerebrovascular diseases and hyperammonemia, etc [61]. Upon the addition of arginine, the emission of the TPP unit enhances gradually, while those of Eu^{3+} changes less, thus making the signals ratiometrically detectable (Figure 1.4c). It is due to the nitrogen atoms in the central pyrazine ring of the TPP unit, which provides sites for binding. On the other hand, the pores in the MOFs are competent in accommodating the arginine. The arginine, therefore, can enter into the MOF and form a hydrogen bond with TPP, thus offering an additional steric hindrance to restrict molecular motions to enhance emission (Figure 1.4d). The emission behavior of Eu^{3+} is less influenced because no interaction is found between Eu^{3+} and arginine. Besides, by replacing the TPP-4COOH ligand with tetracarboxyl-substituted tetraphenylbenzene, the resulting MOF does not possess a response to arginine, further proving the importance of the introduction of an AIE-active TPP unit. The sensor also shows a good selectivity against other amino acids and high sensitivity with a detection limit as low as 15 nM.

1.4 Conclusion

The study of TPP dated back to the mid-nineteenth century, while its real structure was established by Japp and Wilson in 1886. Since that, more studies are focused on synthetic methodologies and medicinal chemistry. It is until 2015 that Tang found TPP to be AIE-active and have merits of easy synthesis, facile medication, good stability, and tunable electronic property, etc. This, therefore, evolves from a variety of functionalities based on tetraphenylpyrazines and makes its researches very attractive.

TPP can be synthesized by cyclization and Suzuki–Miyaura reactions. In the former case, several routes are provided to prepare TPP and its derivatives with mono-, di-, and tetrasubstitutions. For disubstituted TPP, the molecules even with substitutions at different sides can be obtained. By choosing a suitable method, TPP can be synthesized under a very simple and green condition and the purification of TPP can be carried out by recrystallization instead of chromatographic column. The Suzuki–Miyaura reaction can also give tetrasubstituted TPP efficiently and replenish the products that cannot be obtained by the former methods. Encouraged by this, a large amount of desired structures based on TPP can be designed.

TPP-based luminescent materials show different functionalities to indicate their application potentials. Electron-donating group-modified TPPs often show high luminescent efficiencies in the aggregate state and can be utilized to fabricate OLEDs, with EQE approaching theoretic limit. By decorating TPP with an active group, the resulting AIEgen can function as a ratiometric fluorescent sensor to detect H_2S with good selectivity and high sensitivity. Besides, by constructing TPP derivatives with different isomerization effects, a model can be established to elaborate the influence of molecular conjugation and porosity on the sensing properties. TPP can also catch the eyes of researchers in reticular chemistry. For example, the chiral TPP-based organic cage can be obtained from the achiral TPP unit, which can form a host–guest complex with ACQ molecules to construct stable white-light emission materials in the film state. Also, MOFs can be designed based on the TPP unit as ligand, which shows strong emissions due to coordination-induced emission and antenna effect and displays a sensitive and selective ratiometric detection of arginine.

Overall, the researches on TPP are still in an embryonic stage. Many applications are worth being further explored. For example, pyrazines are widely found in natural products and known as antitumor, antibacterial, diuretic, anti-TB, and antidiabetic drugs. Hydroxyl-substituted TPPs are regarded as regulators of estrogen receptors. Thus, it is feasible to develop luminescent drugs and imaging agents to monitor the therapeutic process and life process. On the other hand, functional materials with diversified architectures are very easy to achieve based on TPP. The investigations of TPP-based macrocycles, organic–inorganic coordinated cages, conjugated microporous polymers, covalent organic frameworks, and hydrogen-bonded organic frameworks are still blank. We hope, with this chapter, a picture of the past, now, and future of TPP can be clearly painted and more sparks and opportunities can be motivated to boost the development of TPP-based luminescent materials.

References

1 Zhao, Z., Chen, S., Chan, C. Y. K. et al. (2012) A facile and versatile approach to efficient luminescent materials for applications in organic light-emitting diodes. *Chemistry—An Asian Journal* 7 (3): 484–488.

2 Zhou, J., Liu, Q., Feng, W. et al. (2015) Upconversion luminescent materials: advances and applications. *Chemical Reviews* 115 (1): 395–465.

3 Zhu, X., Su, Q., Feng, W. et al. (2017) Anti-Stokes shift luminescent materials for bio-applications. *Chemical Society Reviews* 46 (4): 1025–1039.

4 Grimsdale, A. C., Chan, K. L., Martin, R. E. et al. (2009) Synthesis of light-emitting conjugated polymers for applications in electroluminescent devices. *Chemical Reviews* 109 (3): 897–1091.

5 Ding, D., Li, K., Liu, B. et al. (2013) Bioprobes based on AIE fluorogens. *Accounts of Chemical Research* 46 (11): 2441–2453.

6 Chen, C., Ou, H., Liu, R. et al. (2020) Regulating the photophysical property of organic/polymer optical agents for promoted cancer phototheranostics. *Advanced Materials* 32 (3): 1806331.

7 Yang, Z., Mao, Z., Xie, Z. et al. (2017) Recent advances in organic thermally activated delayed fluorescence materials. *Chemical Society Reviews* 46 (3): 915–1016.

8 Lee, J. H., Chen, C. H., Lee, P. H. et al. (2019) Blue organic light-emitting diodes: current status, challenges, and future outlook. *Journal of Materials Chemistry C* 7 (20), 5874–5888.

9 Luo, J., Xie, Z., Lam, J. W. Y. et al. (2001) Aggregation-induced emission of 1-methyl-1,2,3,4,5-pentaphenylsilole. *Chemical Communications* 381 (18): 1740–1741.

10 Wang, J., Gu, X., Zhang, P. et al. (2017) Ionization and anion$-\pi^{+}$ interaction: a new strategy for structural design of aggregation-induced emission luminogens. *Journal of the American Chemistry Society* 139 (46): 16974–16979.

11 Wang, Y., Chen, M., Alifu, N. et al. (2017) Aggregation-induced emission luminogen with deep-red emission for through-skull three-photon fluorescence imaging of mouse. *ACS Nano* 11 (10): 10452–10461.

12 Niu, G., Zheng, X., Zhao, Z. et al. (2019) Functionalized acrylonitriles with aggregation-induced emission: structure tuning by simple reaction–condition variation, efficient red emission, and two-photon bioimaging. *Journal of the American Chemistry Society* 141 (38): 15111–15120.

13 Mei, J., Leung, N. L. C., Kwok, R. T. K. et al. (2015) Aggregation-induced emission: together we shine, united we soar! *Chemical Reviews* 115 (21): 11718–11940.

14 Chen, M., Xie, W., Li, D. et al. (2018) Utilizing a pyrazine-containing aggregation-induced emission luminogen as an efficient photosensitizer for imaging-guided two-photon photodynamic therapy. *Chemistry-A European Journal* 24 (62): 16603–16608.

15 Chen, Y., Zhang, W., Zhao, Z. et al. (2018) An easily accessible ionic aggregation-induced emission luminogen with hydrogen-bonding-switchable emission and wash-free imaging ability. *Angewandte Chemie International Edition* 57 (18): 5011–5015.

16 Wang, D., Su, H., Kwok, R. T. K. et al. (2017) Facile synthesis of red/NIR AIE luminogens with simple structures, bright emissions, and high photostabilities, and their applications for specific imaging of lipid droplets and image-guided photodynamic therapy. *Advanced Functional Materials* 27 (46): 1704039.

17 Huang, J., Yang, X., Li, X. et al. (2012) Bipolar AIE-active luminogens comprised of an oxadiazole core and terminal TPE moieties as a new type of host for doped electroluminescence. *Chemical Communications* 48 (77): 9586–9588.

18 Shi, H., Xin, D., Gu, X. et al. (2016) The synthesis of novel AIE emitters with the triphenylethene-carbazole skeleton and para-/meta-substituted arylboron groups and their application in efficient non-doped OLEDs. *Journal of Materials Chemistry C* 4 (6), 1228–1237.

19 Xu, B., Chi, Z., Li, H. et al. (2011) Synthesis and properties of aggregation-induced emission compounds containing triphenylethene and tetraphenylethene moieties. *The Journal of Physical Chemistry C* 115 (35): 17574–17581.

20 Han, T., Zhang, Y. J., Feng, X. et al. (2013) Reversible and hydrogen bonding-assisted piezochromic luminescence for solid-state tetraaryl-buta-1,3-diene. *Chemical Communications* 49 (63): 7049–7051.

21 Yang, Z., Qin, W., Leung, N. L. C. et al. (2016) A mechanistic study of AIE processes of TPE luminogens: intramolecular rotation vs. configurational isomerization. *Journal of Materials Chemistry C* 2016, 4 (1): 99–107.

22 Xiong, J. B., Yuan, Y. X., Wang, L. et al. (2018) Evidence for aggregation-induced emission from free rotation restriction of double bond at excited state. *Organic Letters* 20 (2): 373–376.

23 Qu, D., Yu, T., Yang, Z. et al. Combined aggregation induced emission (AIE), photochromism and photoresponsive wettability in simple dichloro-substituted triphenylethylene derivatives. *Chemical Science* 7 (8): 5302–5306.

24 Li, Z., Dong, Y. Q., Lam, J. W. Y. et al. (2009) Functionalized siloles: versatile synthesis, aggregation-induced emission, and sensory and device applications. *Advanced Functional Materials* 19 (6): 905–917.

25 Nie, H., Chen, B., Zeng, J. et al. (2018) Excellent n-type light emitters based on AIE-active silole derivatives for efficient simplified organic light-emitting diodes. *Journal of Materials Chemistry C* 6 (14): 3690–3698.

26 Liu, G., Chen, D., Kong, L. et al. (2015) Red fluorescent luminogen from pyrrole derivatives with aggregation-enhanced emission for cell membrane imaging. *Chemical Communications* 51 (40): 8555–8558.

27 Li, K., Liu, Y., Li, Y. et al. (2017) 2,5-bis(4-alkoxycarbonylphenyl)-1,4-diaryl-1,4-dihydropyrrolo[3,2-b]pyrrole (AAPP) AIEgens: tunable RIR and TICT characteristics and their multifunctional applications. *Chemical Science* 8 (10): 7528–7267.

28 Nie, H., Hu, K., Cai, Y. et al. (2017) Tetraphenylfuran: aggregation-induced emission or aggregation-caused quenching? *Materials Chemistry Frontiers* 1 (6): 1125–1129.

29 Guo, J., Hu, S., Luo, W. et al. (2017) A novel aggregation-induced emission platform from 2,3-diphenylbenzo[b]thiophene *S*,*S*-dioxide. *Chemical Communications* 53 (9): 1463–1466.

30 Gao, Y., Feng. G., Jiang, T. et al. (2015) Biocompatible nanoparticles based on diketo-pyrrolo-pyrrole (DPP) with aggregation-induced red/NIR emission for in vivo two-photon fluorescence imaging *Advanced Functional Materials* 25 (19): 2857–2866.

31 Zhao, Z., He, B. and Tang, B. Z. (2015) Aggregation-induced emission of siloles. *Chemical Science* 6 (10): 5347–5365.

32 Feng, X., Tong, B., Shen, J. et al. (2010) Aggregation-induced emission enhancement of aryl-substituted pyrrole derivatives. *The Journal of Physical Chemistry B* 114 (50): 16731–16736.

33 Chen, M., Li, L., Nie, H. et al. (2015) Tetraphenylpyrazine-based AIEgens: facile preparation and tunable light emission. *Chemical Science* 6 (3): 1932–1937.

34 Chen, M., Li, L., Wu, H. et al. (2018) Unveiling the different emission behavior of polytriazoles constructed from pyrazine-based AIE monomers by click polymerization. *ACS Applied Materials & Interfaces* 10 (15): 12181–12188.

35 Zhang, J., Liu, Q., Wu, W. et al. (2019) Real-time monitoring of hierarchical self-assembly and induction of circularly polarized luminescence from achiral luminogens. *ACS Nano* 13 (3): 3618–3628.

36 Pan, L., Luo, W., Chen, M. et al. (2016) Tetraphenylpyrazine-based luminogens with aggregation-enhanced emission characteristics: preparation and property. *Chinese Journal of Organic Chemistry* 36 (6): 1316–1324.

37 Han, M., Chen, M., Ebendorff-Heidepriem, H. et al. (2016) An optical fibre sensor for remotely detecting water traces in organic solvents. *RSC Advances* 6 (85): 82186–82190.

38 Chen, M., Hu, X., Liu, J. et al. (2018) Rational design of red AIEgens with a new core structure from non-emissive heteroaromatics. *Chemical Science* 9 (40): 7829–7834.

39 Chen, M., Li, L., Nie, H. et al. (2015) N-type pyrazine and triazole-based luminogens with aggregation-enhanced emission characteristics. *Chemical Communications* 51 (53): 10710–10713.

40 Laurent, A. (1845) Ueber die Einwirkung von Jod auf xanthogensaures Kali. *Journal für praktische Chemie* 36 (1): 352–362.

41 Erdmann, J. (1865) *Ann.* 135: 181.

42 Japp, F. R. and Wilson, W. H. (1886) On ammonia-derivatives of benzoin. *Journal of the Chemical Society* 49: 825–831.

43 Davidson, D., Weiss, M. and Jelling, M. (1937) The action of ammonia on benzoin. *The Journal of Organic Chemistry* 2 (4): 328–334.

44 Dong, Y., Lam, J. W. Y., Qin, A. et al. (2007) Aggregation-induced emissions of tetraphenylethene derivatives and their utilities as chemical vapor sensors and in organic light-emitting diodes. *Applied Physical Letters* 91 (1): 011111.

45 Tamaddon, F. and Tafti, D. A. (2016) $SnCl_2 \cdot H_2O$-catalyzed solvent-free synthesis of α-amino ketones and tetrasubstituted pyrazines. *Synlett* 27 (15): 2217–2220.

46 Tamaddon, F., Tafti, D. A. and Pooramini, F. (2016) An improved synthesis of multi-substituted pyrazines under calalyst- and solvent-free conditions. *Synthesis* 48 (23): 4295–4299.

47 Khafizova, L. O., Shaibakova, M. G. and Dzhemilev, U. M. (2018) A new one-pot synthesis of tetrasubstituted pyrazines by the Ti-catalyzed reaction of aromatic and benzyl-substituted nitriles with $EtAlCl_2$. *Chemistryselect* 3 (41): 11451–11453.

48 Ganji, P. and Leeuwen, P. W. N. M. van (2017) Phosphine supported ruthenium nanoparticle catalyzed synthesis of substituted pyrazines and imidazoles from α-diketones. *The Journal of Organic Chemistry* 82 (3): 1768–1774.

49 Petrosyan, A., Ehlers, P., Reimann, S. et al. (2015) Synthesis of tetraaryl- and tetraalkenylpyrazines by Suzuki–Miyaura reactions of tetrachloropyrazine. *Tetrahedron* 71 (38): 6803–6812.

50 Chen, M., Nie, H., Song, B. et al. (2016) Triphenylamine-functionalized tetraphenylpyrazine: facile preparation and multifaceted functionalities. *Journal of Materials Chemistry C* 4 (14): 2901–2908.

51 Wu, H., Luo, J., Xu, Z. et al. (2020) Uncommon intramolecular charge transfer effect and its potential application in OLED emitters. *Chemical Research in Chinese Universities* 36 (1): 61–67.

52 Wu, H., Pan, Y., Zeng, J. et al. (2019) Novel strategy for constructing high efficiency OLED emitters with excited state quinone-conformation induced planarization process. *Advanced Optical Materials* 7 (18): 1900283.

53 Chen, Y., Zhu, C., Yang, Z. et al. (2013) A ratiometric fluorescent probe for rapid detection of hydrogen sulfide in mitochondria. *Angewandte Chemie International Edition* 52 (6): 1688–1691.

54 Chen, M., Chen, R., Shi, Y. et al. (2018) Malonitrile-functionalized tetraphenylpyrazine: aggregation-induced emission, ratiometric detection of hydrogen sulfide, and mechanochromism. *Advanced Functional Materials* 28 (6): 1704689.

55 Chen, M., Liu, J., Liu, F. et al. (2019) Tailoring the molecular properties with isomerism effect of AIEgens. *Advanced Functional Materials* 29 (37): 1903834.

56 Zhang, G. and Mastalerz, M. (2014) Organic cage compounds-from shape-persistency to function. *Chemical Society Reviews* 43 (6): 1934–1947.

57 Feng, H, Zheng, X. Gu, X. et al. (2018) White-light emission of a binary light-harvesting platform based on an amphiphilic organic cage. *Chemistry of Materials* 30 (4): 1285–1290.

58 Yaghi, O. M., Li, G. and Li, H. (1995) Selective binding and removal of guests in a microporous metal–organic framework. *Nature* 378: 703–706.

59 Li, Q., Ma, Z., Zhang, W. et al. (2016) AIE-active tetraphenylethene functionalized metal–organic framework for selective detection of nitroaromatic explosives and organic photocatalysis. *Chemical Communications* 52 (75): 11284–11287.

60 Tao, C., Chen, B., Liu, X. et al. (2017) A highly luminescent entangled metal–organic framework based on pyridine-substituted tetraphenylethene for efficient pesticide detection. *Chemical Communications* 53 (72): 9975–9978.

61 Yin, H., Wang, X. and Yin, X. (2019) Rotation restricted emission and antenna effect in single metal–organic frameworks. *Journal of the American Chemistry Society* 141 (38): 15166–15173.